THE JOURNAL OF PHYSICAL CHEMISTRY Letters

Letter

pubs.acs.org/JPCL

Proton-Transfer Mechanisms at the Water−ZnO Interface: The Role of Presolvation

Vanessa Quaranta, Matti Hellström,* and Jörg Behler*,†

Lehrstuhl für Theoretische Chemie, Ruhr-Universität Bochum, D-44780 Bochum, Germany

Supporting Information

ABSTRACT: The dissociation of water is an important step in many chemical processes at solid surfaces. In particular, water often spontaneously dissociates near metal oxide surfaces, resulting in a mixture of H_2O, H^+, and OH^- at the interface. Ubiquitous proton-transfer (PT) reactions cause these species to dynamically interconvert, but the underlying mechanisms are poorly understood. Here, we develop and use a reactive high-dimensional neural-network potential based on density functional theory data to elucidate the structural and dynamical properties of the interfacial species at the liquid-water−metal-oxide interface, using the nonpolar ZnO($10\bar{1}0$) surface as a prototypical case. Molecular dynamics simulations reveal that water dissociation and recombination proceed via two types of PT reactions: (i) to and from surface oxide and hydroxide anions ("surface-PT") and (ii) to and from neighboring adsorbed hydroxide ions and water molecules ("adlayer-PT"). We find that the adlayer-PT rate is significantly higher than the surface-PT rate. Water dissociation is, for both types of PT, governed by a predominant presolvation mechanism, i.e., thermal fluctuations that cause the adsorbed water molecules to occasionally accept a hydrogen bond, resulting in a decreased PT barrier and an increased dissociation rate as compared to when no hydrogen bond is present. Consequently, we are able to show that hydrogen bond fluctuations govern PT events at the water−metal-oxide interface in a way similar to that in acidic and basic aqueous bulk solutions.

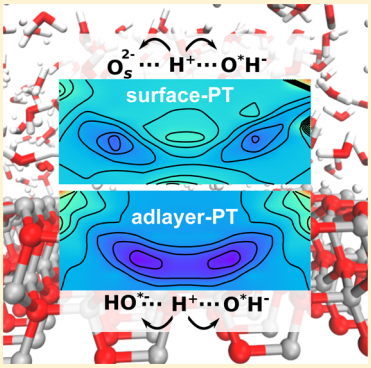

Numerous important processes, e.g., in environmental chemistry, heterogeneous catalysis, and electrochemistry, are governed by the interaction between water and solid surfaces. Consequently, solid−liquid interfaces have received considerable attention in recent years.[1−3] Often these systems exhibit a very dynamical behavior, and water molecules frequently dissociate and recombine,[4−9] resulting in a complicated pattern of molecular (H_2O) and dissociated (H^+ + OH^-) species at the interface. Water dissociation and recombination happen via proton-transfer (PT) reactions to or from the surface, or "within" the interfacial water layers. As a consequence of the liquid solvent, the rates and mechanisms of such PT events are the result of a complex interplay of many phenomena, such as surface diffusion, water exchange, specific interactions with the substrate, and hydrogen bond (HB) fluctuations. Therefore, to date, gaining insights into the origins and mechanisms of PT has been a substantial challenge.

In acidic and basic aqueous solutions, HB fluctuations have been shown to influence the PT rate via so-called *presolvation*, where suitable thermal fluctuations of the HB environment "activate" the proton to be transferred.[10−15] Recently, we suggested that the predominant presolvation mechanism for PT in aqueous NaOH solutions changes in character, from "acceptor-driven" to "donor-driven", when the concentration is increased. The growing number of sodium ions, and the decreasing "liquid-water-like" properties of the solution, cause HB fluctuations around the proton donors (H_2O) to be more important than around the proton acceptors (OH^-), which is the opposite behavior of dilute hydroxide solutions.[16]

The importance of presolvation for PT reactions in inhomogeneous, anisotropic environments, like at solid−liquid interfaces, is still largely unknown. Therefore, because PT is highly relevant for chemistry at surfaces, unravelling possible similarities or differences between concentrated hydroxide solutions and solvated metal-oxide interfaces, where neither the water molecules nor the hydroxide ions are in a "bulk-water"-like environment, is of great interest. To address this issue, for the present work we have chosen zinc oxide (ZnO)[17,18] as the metal oxide, because ZnO−water interfaces are involved in many technological applications, such as biosensors,[19] biomedical devices,[20] and catalysts,[21] and because previous molecular dynamics (MD) studies have suggested an interesting role of the solvent[4,22,23] in this system.

To experimentally probe PT events at interfaces is very challenging if atomic resolution is desired, especially regarding the local environment around molecules before, during, and after the reactions. Computer simulations, on the other hand, provide access to detailed mechanistic information, and MD simulations employing "reactive" potentials, which are able to capture bond-breaking and bond-making events, can be used for such purposes. Extended simulations are of crucial importance, because solvent configurations involving hydrogen bonds or, equally important, lacking hydrogen bonds, to and

Received: February 14, 2017
Accepted: March 15, 2017
Published: March 15, 2017

DOI: 10.1021/acs.jpclett.7b00358
J. Phys. Chem. Lett. 2017, 8, 1476−1483

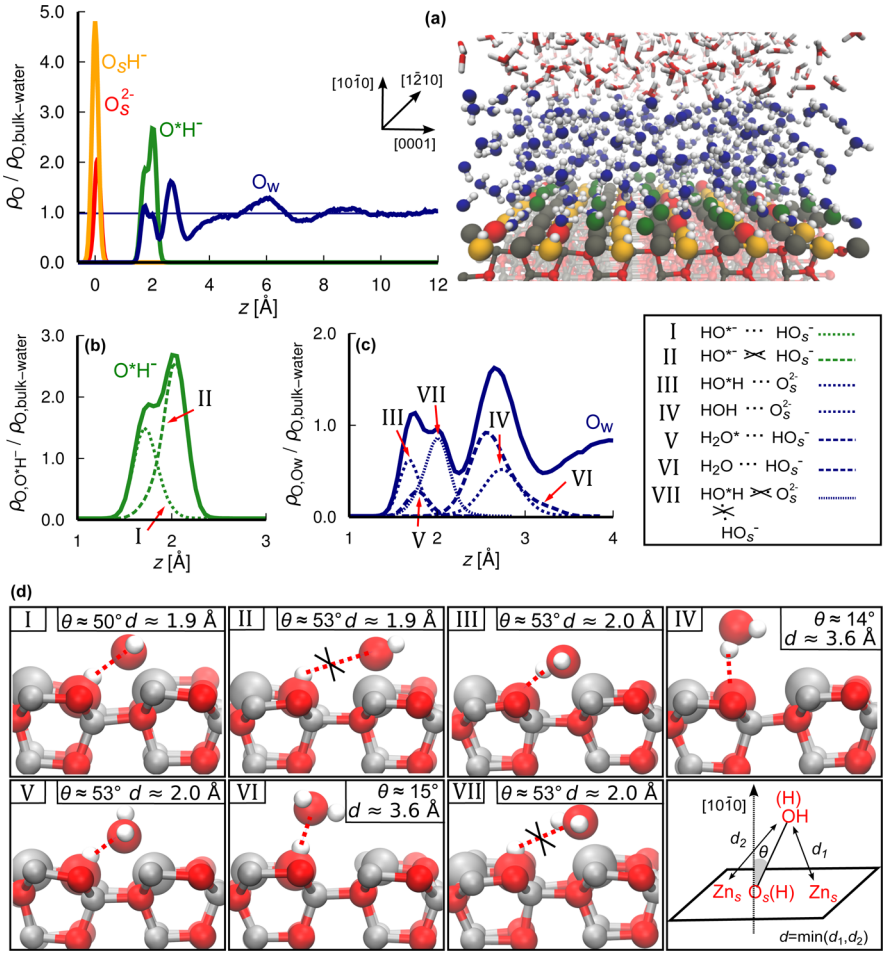

Figure 1. (a) Calculated density profiles of different oxygen species as a function of distance from the ZnO(10$\bar{1}$0) surface and a typical snapshot of the ZnO(10$\bar{1}$0)–liquid-water interface from neural-network-based molecular dynamics (NN-MD) simulations. The data have been normalized to the average oxygen density in bulk liquid water obtained from a corresponding NN-MD simulation. (b, c) Density profiles of O*H$^-$ and O_w (H_2O* and H_2O) divided into different local hydrogen bond complexes. (d) Side view illustrations of the complexes I–VII as well as the definition of the distance d and the angle θ. The atoms used for the geometrical characterization (θ, d) of I–VII are represented by large spheres. The surrounding water molecules and ions have been removed for clarity. The full distributions of θ and d values are given in Figure S3.

from species at the interface are potentially much longer-lived than normal hydrogen bonds in water, and proper equilibration can be ascertained only if other dynamical events, like water exchange processes between the interface and the bulk liquid, are fully captured. First-principles techniques would, in principle, allow for such simulations, but the high computational cost constitutes a severe bottleneck with respect to the system size and the time scales that can be modeled.

MD simulations on the liquid-water–ZnO(10$\bar{1}$0) interface have previously been conducted by Raymand et al.[4] using a reactive classical force-field yielding a hydroxylation level of the surface of about 80–85%. A few years later, ab initio MD simulations were carried out for this system by Tocci and Michaelides[23] as well as by Kharche et al.[24] In these simulations, a smaller fraction of about 50% of the water molecules was found to dissociate at the surface, indicating that both the interaction potential and the simulation size may affect the results. Moreover, Tocci and Michaelides[23] showed that the dissociation of adsorbed water molecules is coupled to fluctuations in the distance to the nearest HB donor. Furthermore, they were able to demonstrate that the presence of liquid water, as compared to monolayer water adsorption, decreases the free-energy "dissociation" barrier and enables a second PT mechanism where the H^+ is transferred between H_2O and OH^- in the adsorbed water layer.

The structure and dynamics of liquid water are particularly challenging to model, although much progress has recently been made for both force-field[5,25] and ab initio simulations.[26] Some recent studies[27,28] have shown that a description of liquid water in good agreement with experimental data can be obtained at the density functional theory (DFT) level using the RPBE functional[29] with D3 dispersion corrections.[30]

Neural network potentials (NNPs)[31−33] belong to the "machine learning" family of interatomic potentials[34] and can reliably represent first-principles-based potential energy surfaces. Here, motivated by previous successful applications of RPBE-D3-based NNPs to explain phenomena like the density anomaly of liquid water[28] and presolvation effects for PT reactions in hydroxide solutions,[16] as well as for studying structural and dynamical properties at the liquid-water–Cu interface,[35,36] we develop a reactive high-dimensional NNP,[37−39] parametrized at the RPBE-D3 level, that is able to describe the water–ZnO(10$\bar{1}$0) interface.

The goal of the present work is to unravel in detail the fundamental mechanisms of PT, to identify the predominant structural features involved, and to characterize the dynamical

DOI: 10.1021/acs.jpclett.7b00358
J. Phys. Chem. Lett. 2017, 8, 1476−1483

behavior of H_2O, H^+, and OH^- species at hydrophilic metal-oxide surfaces using the water−ZnO(10$\bar{1}$0) interface as a model system. We aim to understand PT rates by analyzing the free-energy barriers for different HB environments with respect to accepted and donated hydrogen HBs, the chemical identities of the HB partners, and the dynamical characteristics of the HB environment before and after PT events. These studies yield a comprehensive description of the interfacial region including insights into if and how HB fluctuations, or "presolvation", around the participating species control the rate of water dissociation and recombination.

The MD simulations were performed employing periodic boundary conditions with the ZnO(10$\bar{1}$0) surface modeled as a 12-layer-thick slab in an 8 × 6 supercell, with about 28 Å of water separating periodic images of the slab along the [10$\bar{1}$0] direction. The equilibration procedure is described in the Supporting Information; the production simulations were run for 1 ns with a time step of 0.5 fs in the *NVT* ensemble at 300 K. A snapshot of a part of the system is shown in Figure 1a, and of the entire system in Figure S1. The technical details of the employed NNP, its validation, and the generation of the reference data set used for its parametrization are given in the Supporting Information.

For the analysis, we define each H atom to be "covalently bound" to its nearest O atom. As a result, all O and H atoms form either H_2O molecules or OH^- or O^{2-} ions, where the indicated charges are used for labeling only, as the employed NNP does not depend on any explicit atomic charges but predicts the DFT total energy and forces of the system. A water molecule or hydroxide ion is considered to be "adsorbed" on the surface if the distance between the O atom and the nearest surface Zn_s^{2+} ion is smaller than 2.5 Å, where the subscript "s" indicates a surface ion. Adsorbed oxygen atoms are marked with an asterisk, as in H_2O^* or O^*H^-. Surface oxide anions, O_s^{2-}, can become protonated and form surface hydroxide anions, O_sH^-. Furthermore, we consider $O_dH_d \cdots O_a$ pairs between donor (d) and acceptor (a) to be hydrogen-bonded if the distance $O_dO_a \leq 3.5$ Å and the angle $\angle O_aO_dH_d \leq 30°$.[40]

Figure 1 shows how the ZnO(10$\bar{1}$0) surface modifies the oxygen density ρ_O up to a distance of about 12 Å, where it converges to the corresponding density of the bulk liquid. The surface oxygen atoms consist of 29% O_s^{2-} (red line) and 71% O_sH^- (yellow line), i.e, the equilibrated hydroxylation level lies between the values previously calculated by Raymand et al.[4] (80−85%) and Tocci and Michaelides[23] (50%). Hydroxide ions form only as surface hydroxides (O_sH^-) or adsorbed hydroxide (O^*H^-); no OH^- is found in the bulk solution, i.e., more than 2.5 Å away from the nearest Zn_s^{2+} ion.

A detailed investigation of the interfacial species reveals the presence of different kinds of O^*H^- ions, H_2O^* and solvent H_2O molecules, which are characterized by different HB patterns and geometrical arrangements with respect to the underlying surface (Figure 1b−d). Specifically, we have identified two types of O^*H^- (green line) resulting in the double-peak structure in Figure 1b: type I are O^*H^- accepting an HB from O_sH^-, and type II are O^*H^- that do not accept such HBs (Figure 1b,d). For the water molecules near the interface, there is a larger structural variety: III/IV are H_2O^*/H_2O which donate an HB to O_s^{2-}; V/VI are H_2O^*/H_2O which accept an HB from O_sH^-; and VII are H_2O^* which are not hydrogen-bonded to the surface (Figures 1c and d). The average (shortest) Zn_s^{2+}−O^*H^- distance is 1.9 Å, which is slightly shorter than the average shortest Zn_s^{2+}−O^*H_2 distance

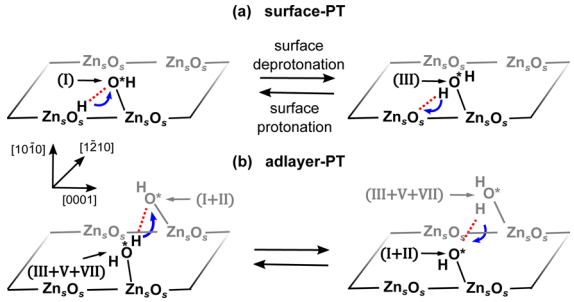

Figure 2. Mechanisms of (a) surface proton transfer and (b) adlayer proton transfer. Surface atoms in the back are drawn in gray. The red dotted line represents a hydrogen bond, while the blue arrow indicates the direction of proton transfer. Formal charges have been omitted for clarity.

of about 2.0 Å. The nonadsorbed bulk water molecules, IV and VI, are located almost "on top" of O_s^{2-}/O_sH^- with the angle θ defined in Figure 1d being only 14−15° on average.

In agreement with previous studies,[23,24] we observe two types of PT reactions occurring at the liquid water−ZnO(10$\bar{1}$0) interface (Figure 2). The first, which involves the surface oxygens, we denote "surface-PT" (Figure 2a):

$$O_sH^- \cdots O^*H^- \rightleftharpoons O_s^{2-} \cdots HO^*H \quad (1)$$

where the forward reaction corresponds to surface deprotonation and the backward reaction to surface protonation. For the forward reaction, we define the O_sH^- to be the "*proton-giver*" and the O^*H^- to be the "*proton-receiver*"; for the backward reaction, H_2O^* is the proton-giver and the O_s^{2-} is the proton-receiver. Here, we reserve the terms "giver" and "receiver" specifically for PT reactions and use the terms "donor" and "acceptor" in the conventional way for any hydrogen bond in the system. Thus, the proton-giver always donates an HB to the proton-receiver, but both the giver and receiver can donate or accept additional HBs from other species.

The second PT mechanism we denote "adlayer-PT" (Figure 2b), and it involves only adsorbed O^*H^- and H_2O^* that are directly neighbored along the [1$\bar{2}$10] direction of the substrate:

$$HO^*H \cdots O^*H^- \rightleftharpoons HO^{*-} \cdots HO^*H \quad (2)$$

Surface-PT reactions are possible only for species I and III (Figure 1d). In contrast, adlayer-PT reactions are possible for all combinations of adsorbed O^*H^- and H_2O^*, i.e., between I/II as receiver and III/V/VII as giver. IV and VI are bulk molecules, which are not part of the adlayer and therefore do not qualify for adlayer-PT, and no dissociation of these molecules has been observed in our simulations.

The proton-transfer free-energy landscape is evaluated as a function of a one-dimensional PT coordinate, δ_{min}, that we determine using the method described in ref 10. Each possible proton receiver, i.e., O_s^{2-} (for surface-PT) or O^*H^- (for both surface-PT and adlayer-PT), is at any given time associated with at most *one* value of δ_{min}. Assuming for example that the receiver O^*H^- accepts two hydrogen bonds, only one of these will be selected as "active" for PT. To ensure this, δ_{min} is calculated as the minimum of the difference of the $O_a \cdots H_d$ and H_d−O_d distances for each donor. When the proton is exactly halfway between the oxygen atoms, $\delta_{min} = 0$ Å. If no hydrogen bond is accepted, no proton transfer can happen and δ_{min} is undefined.

DOI: 10.1021/acs.jpclett.7b00358
J. Phys. Chem. Lett. 2017, 8, 1476−1483

For the Helmholtz free energy we have $\Delta F(\delta_{min}) = -k_B T \ln W(\delta_{min})$, where $W(\delta_{min})$ counts how many times a given receiver (here, O_s^{2-} or O^*H^-), associated with a given value of δ_{min}, appears in the simulation. We plot $\Delta F(\delta_{min})$ for both left- and right-hand sides (LHS and RHS) of different PT reactions, with δ_{min} histogrammed into bins with width 0.1 Å. We further adopt the convention to plot the LHS as $\Delta F(-\delta_{min})$, i.e., at negative δ_{min}-values. The LHS always has O^*H^- as the proton receiver, and the RHS has H_2O^* as the proton giver for both surface-PT and adlayer-PT (eqs 1 and 2). We also evaluate $\Delta F(\delta_{min})$ separately for different hydrogen-bonding environments. In such cases, the HB environment refers to the environment around O^*H^- at the LHS and around H_2O^* at the RHS. The $\Delta F(\pm\delta_{min})$ functions have one minimum ΔF^m_{LHS} at negative δ_{min}, one minimum ΔF^m_{RHS} at positive δ_{min}, and a maximum ΔF^M at $\delta_{min} \approx 0$ Å corresponding to the transition state. The forward and backward PT barriers are $\Delta F^{\ddagger}_{\rightarrow} = \Delta F^M - \Delta F^m_{LHS}$ and $\Delta F^{\ddagger}_{\leftarrow} = \Delta F^M - \Delta F^m_{RHS}$, where forward reactions correspond to the protonation of O^*H^- and backward reactions to the deprotonation of H_2O^*.

Figure 3 shows the calculated free energies of surface-PT and adlayer-PT events. For surface-PT, the surface deprotonation

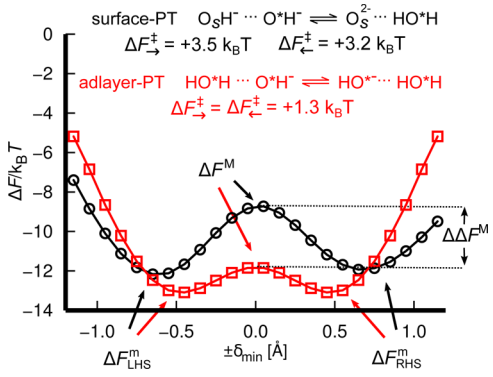

Figure 3. Free-energy landscapes for surface-PT (black) and adlayer-PT (red), with no distinction between different hydrogen-bonding environments.

barrier ($\Delta F^{\ddagger}_{\rightarrow}$ = +3.5 k_BT) is only slightly higher than the surface protonation barrier ($\Delta F^{\ddagger}_{\leftarrow}$ = +3.2 k_BT). The barrier for adlayer-PT ($\Delta F^{\ddagger}_{\rightarrow} = \Delta F^{\ddagger}_{\leftarrow}$ = +1.3 k_BT) is considerably smaller and fully symmetric, because the forward and backward reactions are equivalent. Adlayer-PT species are characterized by a smaller average $H_d \cdots O_a$ distance along the PT coordinate (1.49 Å) as compared to surface-PT species (1.63 Å for the forward reaction and 1.68 Å for the backward reaction), i.e., the proton in adlayer-PT has a shorter distance to travel, and the average HB angle $O_aO_dH_d$ within the PT pair is considerably smaller for adlayer-PT (7°) than for surface-PT (15° and 13°), which could help to explain why the adlayer-PT barrier is smaller than the surface-PT barriers.

Moreover, ΔF is at more negative values for adlayer-PT than surface-PT for the major part of δ_{min}-values, indicating that more proton receivers and givers are in the adlayer-PT than in the surface-PT coordinate. This can easily be rationalized because *all* O^*H^- (I+II) and *all* H_2O^* (III+V+VII) can potentially participate in adlayer-PT reactions, whereas only *some* O^*H^- (I) and *some* H_2O^* (III) can participate in surface-PT reactions. We emphasize that a receiver at any given point in time can belong to only one of the two PT types (or neither of them), depending what kind of HB donor is "active" (i.e., the donor for which δ_{min} is calculated). We find that, of all O^*H^-, 12% qualify for surface-PT, 33% qualify for adlayer-PT, and the rest cannot be classified as any of these two mechanisms, which happens whenever the "active" donor is another O^*H^- or a solvent H_2O molecule, or if there is no donor. Similarly, of all H_2O^*, 25% qualify for surface-PT, 78% qualify for adlayer-PT, and 6% remain unclassified. The fractions add up to more than 100%, because H_2O^* has two donors that can simultaneously participate in different PT mechanisms.

We use the calculated ΔF^M-values, i.e., the ΔF-value at the transition-state (see Figure 3), as a proxy for the PT rate, and calculate relative rates, including both forward and backward reactions, between two mechanisms i and j as

$$\frac{r_i}{r_j} = \frac{\exp(-\Delta F_i^M/k_BT)}{\exp(-\Delta F_j^M/k_BT)} = \exp(\Delta\Delta F^M/k_BT) \quad (3)$$

as also done in ref 16. This treatment is based on transition-state theory and assumes that the "transmission coefficients" are roughly equal for the different mechanisms involved. The forward and backward rates can be assumed to be equal because we are sampling an equilibrium distribution, and if the forward and backward reactions are different, then

$$\frac{r_{i,\rightarrow}}{r_{j,\rightarrow}} = \frac{r_{i,\leftarrow}}{r_{j,\leftarrow}} = \frac{r_i}{r_j} \quad (4)$$

Using the above equations, so-called proton "rattling" events, i.e., events where a proton quickly jumps back and forth between two oxygen atoms before settling on one of them, also contribute to the overall PT rate. We focus on relative rates, as opposed to absolute rates, to minimize the influence of proton rattling, and because nuclear quantum effects, which have been demonstrated to lower PT barriers,[10] have not been considered in the present study but are left for future work. For the two mechanisms in Figure 3, we find $\frac{r_{adlayer\text{-}PT}}{r_{surface\text{-}PT}}$ = 22, suggesting that for every surface-PT event, there are 22 adlayer-PT events.

The global free-energy landscapes in Figure 3 include all of the possible HB environments around the proton receivers and givers. Now, as the details of the HB network may play an important role, we analyze the influence of the specific local environments. In the Supporting Information (Figure S4), we explore the PT barriers and rates based on the chemical *identities* (O^*H^-, H_2O^*, H_2O) of the different HB partners around the proton givers and receivers and illustrate, for example, how some O^*H^- and some H_2O^* are "PT-ambivalent" and can participate in PT events of both mechanisms. Here, we focus on the local environment around the proton receivers O^*H^- and the proton givers H_2O^* by means of the *number* of donated (D) and accepted (A) HBs. For each PT mechanism there are two environmental quantities $D(O^*H^-)$ and $A(O^*H^-)$ for the forward reaction, and two environmental quantities $D(H_2O^*)$ and $A(H_2O^*)$ for the backward reaction. For surface-PT, it is always the case that $D(O_sH^-) = 1$ for the forward reaction, and $A(O_s^{2-}) = 1$ for the backward reaction, so these quantities are not further considered here. The time evolution of the average value of all these parameters, before and after PT events according to both mechanisms, is given in Figure S5, showing that the average HB environments change both before and after the PT events.

The PT free-energy landscapes for the all occurring values of $D(O^*H^-)$, $D(H_2O^*)$, $A(O^*H^-)$, and $A(H_2O^*)$ are plotted in

DOI: 10.1021/acs.jpclett.7b00358
J. Phys. Chem. Lett. 2017, 8, 1476−1483

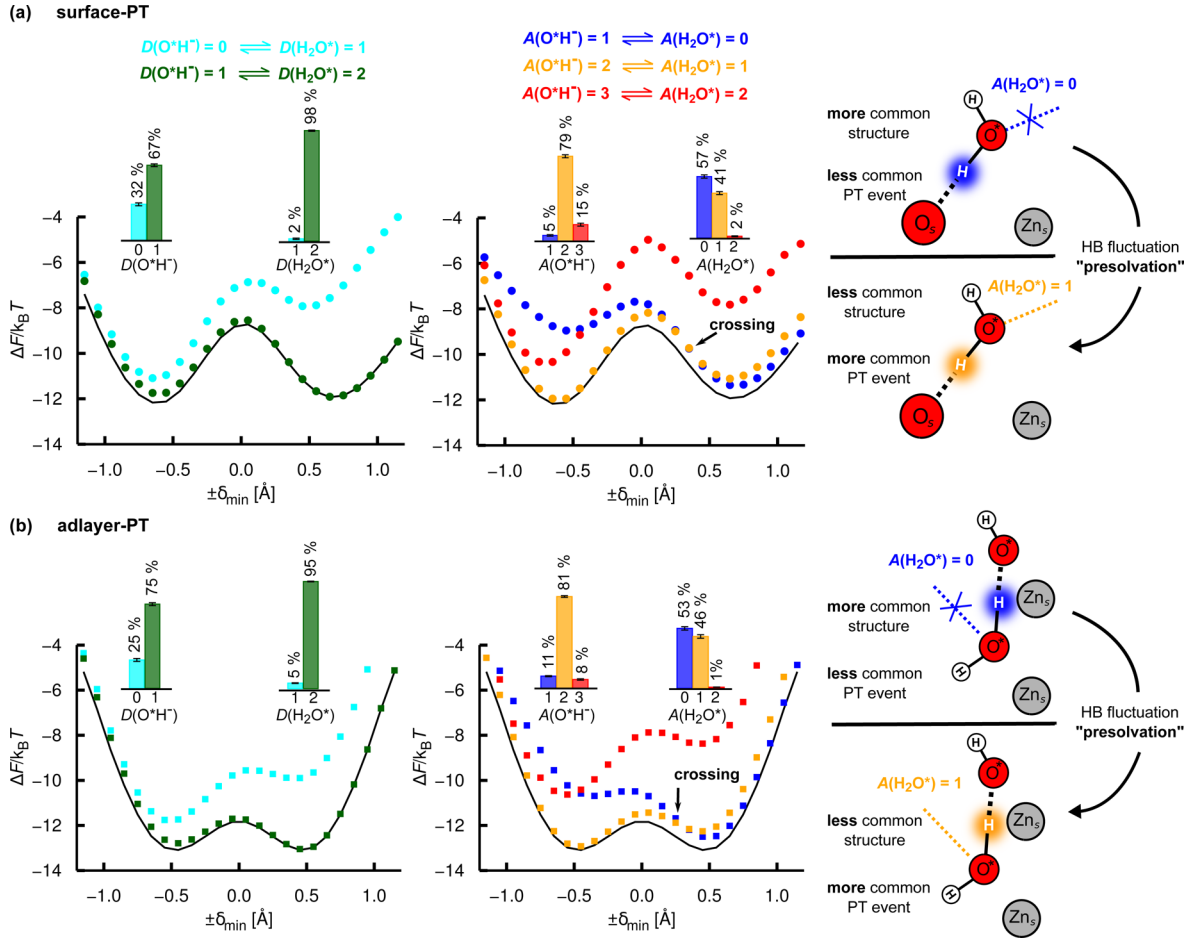

Figure 4. Free-energy landscapes as a function of δ_{min} for (a) surface-PT and (b) adlayer-PT, for specific values of $D(O^*H^-)$, $D(H_2O^*)$ (cyan, green) and $A(O^*H^-)$, $A(H_2O^*)$ (blue, orange, red). D is the number of donated and A the number of accepted hydrogen bonds. The global barriers (from Figure 3) are represented by thin lines. The histogram error bars have been calculated by block-averaging over 10 equally sized portions of the trajectory as 2.26 × (standard error of the mean). The predominant presolvation mechanisms for the water dissociation reactions are given in the schematic illustrations. The main features of the above graphs are tabulated in Tables S2 and S3.

Figure 4, together with their "equilibrium distributions" (histograms). The equilibrium distributions give the fractions of different environments that occur for a particular PT mechanism irrespective of the value of δ_{min}. Here, we treat the number of donated HBs independently of the number of accepted HBs; Figure S6 instead shows the same free-energy landscapes for all combinations of both D and A, but the qualitative results below do not depend on whether D and A are treated independently or in combination (see the Supporting Information).

We discern what kind of HB fluctuations constitute "predominant presolvation mechanisms" for PT by checking whether all of the following three conditions[16] are fulfilled:

1. The fluctuation happens from the most stable HB environment i to a less stable HB environment j, so that the equilibrium concentration $N_j < N_i$.
2. The PT barrier becomes smaller as a result of the fluctuation, i.e., $\Delta F^{\ddagger}(j) < \Delta F^{\ddagger}(i)$.
3. The PT rate is greater in environment j than in i, i.e., $r_j > r_i$, or, equivalently, $\Delta F^{M}(j) < \Delta F^{M}(i)$.

If condition 2 is fulfilled, then the fluctuation from i to j will give an increased average PT rate as compared to a system where such a fluctuation could not occur, and the fluctuation could therefore be thought of as presolvation that aids the PT reaction. However, if the HB environment j is considerably less stable than i, i.e., if the destabilization in condition 1 is large, then the fluctuation would happen only rarely and the presolvation mechanism would barely contribute to the PT rate. In order to determine what kind of HB fluctuations constitute *predominant* presolvation mechanisms, we apply condition 3, which is fulfilled whenever the decrease of the PT barrier (condition 2) is greater than the decrease in stability (condition 1) when going from i to j. Condition 3 implies that *more* PT events occur in the less stable environment than in the more stable environment. This can graphically be seen as the two free-energy landscapes for i and j "crossing" between the maximum and the minimum.

Similar to what we previously reported for aqueous hydroxide solutions,[16] we find that the local HB environment influences the PT barriers in opposite ways for O^*H^- and H_2O^* (Figure 4 and Tables S2 and S3). The PT barrier is smaller if O^*H^- donates more HBs and if it accepts fewer HBs. For H_2O^* the situation is opposite: the PT barrier becomes smaller if H_2O^* donates fewer HBs and accepts more HBs. This helps to rationalize why the adlayer-PT barrier is smaller than the two surface-PT barriers in Figure 3: the weighted averages of the equilibrium distribution histograms in Figure 4 are, for surface-PT (adlayer-PT), $D(O^*H^-)$ = 0.67 (0.75),

DOI: 10.1021/acs.jpclett.7b00358
J. Phys. Chem. Lett. 2017, 8, 1476−1483

$D(H_2O^*)$ = 1.98 (1.95), $A(O^*H^-)$ = 2.09 (1.97), and $A(H_2O^*)$ = 0.44 (0.48).

In general, we find that HB fluctuations can have a significant impact on the PT barriers. For example, 98% of H_2O^* in the surface-PT coordinate (type III) donate hydrogen bonds through both the H atoms; one to O_s^{2-} and the other to another O^*H^-, H_2O^*, or solvent H_2O. If the second donated HB is lost, so that only the HB to O_s^{2-} remains, the PT barrier for the surface-PT mechanism decreases from +3.4 k_BT to only +1.0 k_BT, and this kind of hydrogen bond fluctuation thus enhances the overall PT rate (conditions 1 and 2 are fulfilled). However, despite the smaller barrier, most PT events still proceed with the donated HB being intact (seen in Figure 4a from the relative positions of the two ΔF^M-values), because H_2O^* of type III rarely donate only one HB. This means that condition 3 is *not* fulfilled, and the fluctuation from $D(H_2O^*)$ = 2 to $D(H_2O^*)$ = 1 qualifies as a presolvation mechanism, but not as a *predominant* presolvation mechanism. For the forward surface-PT reaction, 67% of O^*H^- donate an HB, and the barrier to receive a proton is +3.2 k_BT. If the donated HB is lost, the barrier increases to +4.2 k_BT, so fluctuations wherein O^*H^- loses its donated HB decrease the overall PT rate (conditions 2 and 3 are not fulfilled). The relative rate $\frac{r_{\text{surface-PT}}(D(O^*H^-)=1 \rightleftharpoons D(H_2O^*)=2)}{r_{\text{surface-PT}}(D(O^*H^-)=0 \rightleftharpoons D(H_2O^*)=1)}$ = 4.9, i.e., 4.9 times as many PT events occur in which the donated HB is intact as compared to when it is broken.

For adlayer-PT (Figure 4b), the PT barriers are smaller than for surface-PT, but the same trends are found with respect to the hydrogen bond donation numbers of O^*H^- and H_2O^*. The relative rate $\frac{r_{\text{adlayer-PT}}(D(O^*H^-)=1 \rightleftharpoons D(H_2O^*)=2)}{r_{\text{adlayer-PT}}(D(O^*H^-)=0 \rightleftharpoons D(H_2O^*)=1)}$ = 8.1, meaning that, whether or not O^*H^- and H_2O^* donate HBs influences the rate of adlayer-PT reactions more than it influences the rate of surface-PT reactions.

In the preceding example, the PT rates for both surface-PT and adlayer-PT were the greatest for $D(O^*H^-) = 1 \rightleftharpoons D(H_2O^*) = 2$, which is consistent with the equilibrium distributions; $D(O^*H^-)$ = 1 is more common than $D(O^*H^-)$ = 0, and $D(H_2O^*)$ = 2 is more common than $D(H_2O^*)$ = 1 (Figure 4). However, for the HB acceptance numbers A, there are some *in*consistencies between the equilibrium distributions and the relative rates.

Figure 4a shows that for the backward surface-PT reaction, 57% of proton givers H_2O^* have A = 0 and 41% have A = 1. Despite this, a greater PT rate (i.e., more overall PT events) is found for A = 1; the relative rate $\frac{r_{\leftarrow}(A(H_2O^*)=1)}{r_{\leftarrow}(A(H_2O^*)=0)}$ = 1.6 [and the corresponding relative equilibrium concentrations $\frac{N(A(H_2O^*)=1)}{N(A(H_2O^*)=0)} = \frac{41}{57}$ = 0.72]. Thus, conditions 1, 2, and 3 are fulfilled, so the water dissociation mechanism via surface-PT, i.e., surface protonation, proceeds via a predominant presolvation mechanism, wherein the proton giver H_2O^* accepts an additional hydrogen bond, thus changing from $A(H_2O^*)$ = 0 to $A(H_2O^*)$ = 1 before the proton is transferred. This is schematically indicated in the right part of Figure 4a.

The PT rate for the forward surface-PT reaction also depends on the number of accepted hydrogen bonds, $A(O^*H^-)$. Here, however, the maximum PT rate is obtained for $A(O^*H^-)$ = 2, which is also the most frequently occurring value, and there is therefore no predominant presolvation mechanism with respect to $A(O^*H^-)$. However, a fluctuation from $A(O^*H^-)$ = 2 to $A(O^*H^-)$ = 1 would decrease the PT barrier, fulfilling conditions 1 and 2 and increasing the average PT rate [similar to the fluctuation from $D(H_2O^*)$ = 2 to $D(H_2O^*)$ = 1]. Interestingly, because PT barriers are lowered for O^*H^- accepting fewer hydrogen bonds, a greater PT rate is obtained for $A(O^*H^-)$ = 1 than for $A(O^*H^-)$ = 3, despite $A(O^*H^-)$ = 3 being more common [the relative rate $\frac{r_{\rightarrow}(A(O^*H^-)=1)}{r_{\rightarrow}(A(O^*H^-)=3)}$ = 14.8, whereas $\frac{N(A(O^*H^-)=1)}{N(A(O^*H^-)=3)} = \frac{5}{15}$ = 0.33]. However, because the most stable HB environment is $A(O^*H^-)$ = 2, condition 1 is not fulfilled and we do not consider the fluctuation from $A(O^*H^-)$ = 1 to $A(O^*H^-)$ = 3 to constitute a predominant presolvation mechanism.

As was the case for HB donation numbers, the different adlayer-PT free-energy landscapes for different HB acceptance numbers (Figure 4b) resemble those of surface-PT (Figure 4a). For adlayer-PT, there is also a predominant presolvation mechanism with respect to $A(H_2O^*)$, with the relative rate $\frac{r_{\leftarrow}(A(H_2O^*)=1)}{r_{\leftarrow}(A(H_2O^*)=0)}$ = 2.4, which is greater than the corresponding relative rate of 1.6 that we found for surface-PT.

For both the number of donated and accepted hydrogen bonds, the hydrogen bond fluctuations thus have greater impact on the rate of adlayer-PT than the rate of surface-PT.

Tocci and Michaelides also reported, on the basis of ab initio MD simulations, a kind of presolvation mechanism for the water dissociation reaction at ZnO($10\bar{1}0$), but only for the surface-PT coordinate.[23] They found that if H_2O^* accepts an HB from another water molecule, then thermal fluctuations could shorten the HB and decrease the barrier for PT to O_s^{2-}. Our approach differs from their analysis in that we do not focus on the HB distance but instead on whether the HB is present at all. The two kinds of analyses are complementary to each other and provide different perspectives on the water dissociation reaction at ZnO surfaces. Here, we find that not only is the barrier decreased when H_2O^* accepts an HB, but the overall *rate* of PT is greater for H_2O^* that accept HBs as compared to those that do not, despite the majority of H_2O^* not accepting HBs.

This result for the proton-giving H_2O^* has some striking similarities to our previous work about PT in NaOH solutions.[16] In dilute NaOH solutions, HB fluctuations around the proton-*receiver* OH^-(aq) were found to mainly affect the PT rate, but in more concentrated solutions, close to all H_2O are coordinated to at least one Na^+, which means that most H_2O molecules in such solutions accept fewer HBs, because the Na^+ "blocks" the volume that a potential HB-donor would need. For such concentrated solutions, HB fluctuations around the proton-*giver* H_2O (coordinated to Na^+) were found to be more important for PT. Specifically the kind of fluctuation that increases the number of HBs that H_2O accepts, just as we see in the present work for the liquid-water−ZnO($10\bar{1}0$) interface, where the potential proton-givers H_2O^* are coordinated to a cation (Zn_s^{2+}) and accept fewer HBs than in bulk water solution. It thus seems that the great importance of hydrogen-bonding fluctuations around proton-giving water molecules whenever the water molecule is coordinated to a cation is a general phenomenon.

In conclusion, we have reported a detailed study of the structural organization and proton-transfer reactions occurring at the water−ZnO($10\bar{1}0$) interface by means of extended reactive molecular dynamics simulations, where the underlying potential energy surface has been developed within the neural-

DOI: 10.1021/acs.jpclett.7b00358
J. Phys. Chem. Lett. 2017, 8, 1476−1483

network machine-learning approach. Two types of PT reactions occur at the interface: "surface-PT" that involves the surface oxygens and "adlayer-PT" that occurs between adsorbed water and hydroxide. Adlayer-PT reactions are favored, i.e., have greater PT rate than surface-PT, because the adlayer-PT barriers are smaller, and there are no particular geometrical restrictions on the participating species, unlike the case of surface-PT. For both types of PT coordinates, water molecules dissociate via a predominant "presolvation" mechanism characterized by hydrogen-bond fluctuations surrounding the proton-giving water molecule, which has many similarities to the presolvation that precedes PT during water dissociation in NaOH(aq) solutions at high concentrations.[16] In contrast, for water recombination events, HB fluctuations around the proton-receiving hydroxide ion play less of a role. We find that HB fluctuations influence the rate of adlayer-PT more than the rate of surface-PT. We believe these findings represent important progress for the modeling of water−metal-oxide interfaces, as well as the understanding on proton-transfer reactions at such interfaces with possible implications on metal-oxide supported heterogeneous catalysis.

■ ASSOCIATED CONTENT

Supporting Information

The Supporting Information is available free of charge on the ACS Publications website at DOI: 10.1021/acs.jpclett.7b00358.

Snapshot (Cartesian coordinates) of the system (ZIP)

Detailed description of the method with a validation section of the neural network potential, supplementary results, comparison with free-energy landscapes and density profiles calculated with ab initio MD (PDF)

■ AUTHOR INFORMATION

Corresponding Authors

*E-mail: matti.hellstroem@theochem.rub.de.

*E-mail: joerg.behler@uni-goettingen.de.

ORCID

Vanessa Quaranta: 0000-0001-5098-3234

Matti Hellström: 0000-0003-3053-5658

Jörg Behler: 0000-0002-1220-1542

Present Address

†J.B.: Institut für Physikalische Chemie, Georg-August-Universität Göttingen, Tammannstraße 6, D-37077 Göttingen, Germany.

Notes

The authors declare no competing financial interest.

■ ACKNOWLEDGMENTS

This work was supported by the Cluster of Excellence RESOLV (EXC 1069) funded by the Deutsche Forschungsgemeinschaft, the DFG Heisenberg fellowship Be3264/6-1, and the DFG Heisenberg professorship Be3264/11-1. The authors thank Tobias Morawietz for providing the geometries of bulk water and Suresh Kondati Natarajan for useful discussions.

■ REFERENCES

(1) Henderson, M. A. The interaction of water with solid surfaces: fundamental aspects revisited. *Surf. Sci. Rep.* **2002**, *46*, 1−308.

(2) Carrasco, J.; Hodgson, A.; Michaelides, A. A molecular perspective of water at metal interfaces. *Nat. Mater.* **2012**, *11*, 667−674.

(3) Björneholm, O.; Hansen, M. H.; Hodgson, A.; Liu, L.-M.; Limmer, D. T.; Michaelides, A.; Pedevilla, P.; Rossmeisl, J.; Shen, H.; Tocci, G.; et al. Water at Interfaces. *Chem. Rev.* **2016**, *116*, 7698−7726.

(4) Raymand, D.; van Duin, A. C. T.; Goddard, W. A., III; Hermansson, K.; Spångberg, D. Hydroxylation Structure and Proton Transfer Reactivity at the Zinc Oxide-Water Interface. *J. Phys. Chem. C* **2011**, *115*, 8573−8579.

(5) Raju, M.; Kim, S.-Y.; van Duin, A. C. T.; Fichthorn, K. A. ReaxFF Reactive Force Field Study of the Dissociation of Water on Titania Surfaces. *J. Phys. Chem. C* **2013**, *117*, 10558−10572.

(6) Wood, B. C.; Schwegler, E.; Choi, W. I.; Ogitsu, T. Hydrogen-Bond Dynamics of Water at the Interface with InP/GaP(001) and the Implications for Photoelectrochemistry. *J. Am. Chem. Soc.* **2013**, *135*, 15774−15783.

(7) Sato, R.; Ohkuma, S.; Shibuta, Y.; Shimojo, F.; Yamaguchi, S. Proton Migration on Hydrated Surface of Cubic ZrO_2: Ab initio Molecular Dynamics Simulation. *J. Phys. Chem. C* **2015**, *119*, 28925−28933.

(8) Farnesi Camellone, M.; Negreiros Ribeiro, F.; Szabová, L.; Tateyama, Y.; Fabris, S. Catalytic Proton Dynamics at the Water/Solid Interface of Ceria-Supported Pt Clusters. *J. Am. Chem. Soc.* **2016**, *138*, 11560−11567.

(9) Hussain, H.; Tocci, G.; Woolcot, T.; Torrelles, X.; Pang, C. L.; Humphrey, D. S.; Yim, C. M.; Grinter, D. C.; Cabailh, G.; Bikondoa, O.; et al. Structure of a model TiO_2 photocatalytic interface. *Nat. Mater.* **2016**, DOI: 10.1038/nmat4793.

(10) Tuckerman, M. E.; Marx, D.; Parrinello, M. The nature and transport mechanism of hydrated hydroxide ions in aqueous solution. *Nature* **2002**, *417*, 925−929.

(11) Tuckerman, M. E.; Chandra, A.; Marx, D. Structure and Dynamics of OH^-(aq). *Acc. Chem. Res.* **2006**, *39*, 151−158.

(12) Berkelbach, T. C.; Lee, H.-S.; Tuckerman, M. E. Concerted Hydrogen-Bond Dynamics in the Transport Mechanism of the Hydrated Proton: A First-Principles Molecular Dynamics Study. *Phys. Rev. Lett.* **2009**, *103*, 238302.

(13) Marx, D.; Chandra, A.; Tuckerman, M. E. Aqueous Basic Solutions: Hydroxide Solvation, Structural Diffusion, and Comparison to the Hydrated Proton. *Chem. Rev.* **2010**, *110*, 2174−2216.

(14) Biswas, R.; Tse, Y.-L. S.; Tokmakoff, A.; Voth, G. A. Role of Presolvation and Anharmonicity in Aqueous Phase Hydrated Proton Solvation and Transport. *J. Phys. Chem. B* **2016**, *120*, 1793−1804.

(15) McDonnell, M. T.; Xu, H.; Keffer, D. J. Ab Initio Molecular Dynamics Simulations of an Excess Proton in a Triethylene Glycol-Water Solution: Solvation Structure, Mechanism, and Kinetics. *J. Phys. Chem. B* **2016**, *120*, 5223−5242.

(16) Hellström, M.; Behler, J. Concentration-Dependent Proton Transfer Mechanisms in Aqueous NaOH Solutions: From Acceptor-Driven to Donor-Driven and Back. *J. Phys. Chem. Lett.* **2016**, *7*, 3302−3306.

(17) Özgür, Ü.; Alivov, Y. I.; Liu, C.; Teke, A.; Reshchikov, M. A.; Doğan, S.; Avrutin, V.; Cho, S.-J.; Morkoç, H. A comprehensive review of ZnO materials and devices. *J. Appl. Phys.* **2005**, *98*, 041301.

(18) Wöll, C. The chemistry and physics of zinc oxide surfaces. *Prog. Surf. Sci.* **2007**, *82*, 55−120.

(19) Tereshchenko, A.; Bechelany, M.; Viter, R.; Khranovskyy, V.; Smyntyna, V.; Starodub, N.; Yakimova, R. Optical biosensors based on ZnO nanostructures: advantages and perspectives. A review. *Sens. Actuators, B* **2016**, *229*, 664−677.

(20) Rasmussen, J. W.; Martinez, E.; Louka, P.; Wingett, D. G. Zinc oxide nanoparticles for selective destruction of tumor cells and potential for drug delivery applications. *Expert Opin. Drug Delivery* **2010**, *7*, 1063−1077.

(21) Maeda, K.; Domen, K. Photocatalytic Water Splitting: Recent Progress and Future Challenges. *J. Phys. Chem. Lett.* **2010**, *1*, 2655−2661.

(22) große Holthaus, S.; Köppen, S.; Frauenheim, T.; Colombi Ciacchi, L. Atomistic Simulations of the ZnO$(1\bar{2}10)$/Water Interface: A Comparison between First-Principles, Tight-Binding, and Empirical Methods. *J. Chem. Theory Comput.* **2012**, *8*, 4517−4526.

(23) Tocci, G.; Michaelides, A. Solvent-Induced Proton Hopping at a Water-Oxide Interface. *J. Phys. Chem. Lett.* **2014**, *5*, 474−480.
(24) Kharche, N.; Hybertsen, M. S.; Muckerman, J. T. Computational investigation of structural and electronic properties of aqueous interfaces of GaN, ZnO, and a GaN/ZnO alloy. *Phys. Chem. Chem. Phys.* **2014**, *16*, 12057−12066.
(25) Cisneros, G. A.; Wikfeldt, K. T.; Ojamäe, L.; Lu, J.; Xu, Y.; Torabifard, H.; Bartók, A. P.; Csányi, G.; Molinero, V.; Paesani, F. Modeling Molecular Interactions in Water: From Pairwise to Many-Body Potential Energy Functions. *Chem. Rev.* **2016**, *116*, 7501−7528.
(26) Gillan, M. J.; Alfè, D.; Michaelides, A. Perspective: How good is DFT for water? *J. Chem. Phys.* **2016**, *144*, 130901.
(27) Forster-Tonigold, K.; Groß, A. Dispersion corrected RPBE studies of liquid water. *J. Chem. Phys.* **2014**, *141*, 064501.
(28) Morawietz, T.; Singraber, A.; Dellago, C.; Behler, J. How van der Waals interactions determine the unique properties of water. *Proc. Natl. Acad. Sci. U. S. A.* **2016**, *113*, 8368−8373.
(29) Hammer, B.; Hansen, L. B.; Nørskov, J. K. Improved adsorption energetics within density-functional theory using revised Perdew-Burke-Ernzerhof functionals. *Phys. Rev. B: Condens. Matter Mater. Phys.* **1999**, *59*, 7413−7421.
(30) Grimme, S.; Antony, J.; Ehrlich, S.; Krieg, H. A consistent and accurate ab initio parametrization of density functional dispersion correction (DFT-D) for the 94 elements H-Pu. *J. Chem. Phys.* **2010**, *132*, 154104.
(31) Blank, T. B.; Brown, S. D.; Calhoun, A. W.; Doren, D. J. Neural network models of potential energy surfaces. *J. Chem. Phys.* **1995**, *103*, 4129−4137.
(32) Handley, C. M.; Popelier, P. L. A. Potential Energy Surfaces Fitted by Artificial Neural Networks. *J. Phys. Chem. A* **2010**, *114*, 3371−3383.
(33) Behler, J. Neural network potential-energy surfaces in chemistry: a tool for large-scale simulations. *Phys. Chem. Chem. Phys.* **2011**, *13*, 17930−17955.
(34) Behler, J. Perspective: Machine Learning Potentials for Atomistic Simulations. *J. Chem. Phys.* **2016**, *145*, 170901.
(35) Natarajan, S. K.; Behler, J. Neural network molecular dynamics simulations of solid-liquid interfaces: water at low-index copper surfaces. *Phys. Chem. Chem. Phys.* **2016**, *18*, 28704−28725.
(36) Kondati Natarajan, S.; Behler, J. Self-Diffusion of Surface Defects at Copper-Water Interfaces. *J. Phys. Chem. C* **2017**, *121*, 4368−4383.
(37) Behler, J.; Parrinello, M. Generalized Neural-Network Representation of High-Dimensional Potential-Energy Surfaces. *Phys. Rev. Lett.* **2007**, *98*, 146401.
(38) Behler, J. Representing potential energy surfaces by high-dimensional neural network potentials. *J. Phys.: Condens. Matter* **2014**, *26*, 183001.
(39) Behler, J. Constructing high-dimensional neural network potentials: A tutorial review. *Int. J. Quantum Chem.* **2015**, *115*, 1032−1050.
(40) Luzar, A.; Chandler, D. Effect of Environment on Hydrogen Bond Dynamics in Liquid Water. *Phys. Rev. Lett.* **1996**, *76*, 928−931.

DOI: 10.1021/acs.jpclett.7b00358
J. Phys. Chem. Lett. 2017, 8, 1476−1483